Journal of Ceramic Processing Research. Vol. 7, No. 3, pp. 275~279 (2006)

J O U R N A L O F
Ceramic Processing Research

Mechanical, electrical and wear properties of Cu-TiB_2 nanocomposites fabricated by MA-SHS and SPS

Dae-Hwan Kwon, Thuy Dang Nguyen, Khoa Xuan Huynh, Pyuck-Pa Choi, Myung-Gyu Chang, Young-Jin Yum[a], Ji-Soon Kim* and Young-Soon Kwon

School of Materials Science & Engineering, Research Center for Machine Parts and Materials Processing, University of Ulsan, San 29 Mugeo-dong, Nam-gu, Ulsan 680-749, Korea

[a]School of Mechanical and Automotive Engineering, Research Center for Machine Parts and Materials Processing, University of Ulsan, San 29 Mugeo-dong, Nam-gu, Ulsan 680-749, Korea

Cu-TiB_2 nanocomposite powders were obtained by means of a combination of mechanical treatment and combustion reaction. Spark plasma sintering (SPS) was used to inhibit grain growth and thereby obtain fully dense Cu-TiB_2 sintered bodies with a nanocomposite structure. The phases of the synthesized product were identified using X-ray diffraction and results showed only Cu and TiB_2, with no other phases existing in the product. The particle size of self-propagating high-temperature synthesized powder was smaller than 250 nm. Mechanical and electrical properties were investigated after SPS at 650 °C for 30 minutes, the electrical conductivity decreased from 75 to 54% International Annealed Copper Standard (IACS) with the TiB_2 content increased from 2.5 to 10 wt.%. while the hardness increased from 56 to 97 H_RB. In addition, the tensile strength and wear resistance of the composites increased as the TiB_2 content increased.

Key words: Cu-TiB_2 composite, slef-propagating high-temperature synthesis, spark-plasma sintering, wear resistance, tensile strength.

Introduction

Copper and copper-based alloys are widely used as electric and electrode materials due to their good conductivity. However, in the case of precipitation hardened copper alloys (such as Cu-Zr and Cu-Cr) with high strength, there is a problem that the mechanical property decreases rapidly due to the presence of a coarse precipitate phase at high temperature. This problem limits the application of copper alloy in electrical and resistance welding applications [1-3].

There have been several efforts to develop copper alloys which exhibit good mechanical properties even at elevated temperatures. Copper-base metal matrix composites (MMC) with reinforcing ceramic particles such as oxides, borides and carbides were developed as electrode materials because the ceramic particles are stable at high temperatures [4-12]. TiB_2 was also found to be a potential candidate for reinforcement of the copper alloy because of its high melting point, hardness, thermal conductivity as well as electrical conductivity [13].

Recently, much attention has been focused on self-propagating high-temperature synthesis (SHS), one of the in-situ processes to produce metal matrix composites (MMCs) [14]. SHS is extremely attractive due to its short time of synthesis, low energy consumption and the high purity of products. Spark plasma sintering (SPS) is a newly-developed process which makes sintering of high quality materials in short periods possible by DC pulse charging between powder particles with relatively high sintering pressures [15]. SPS systems offer many advantages (e.g. rapid sintering, less sintering additives, uniform sintering, low running cost, easy operation) over conventional systems like hot press (HP) sintering, hot isostatic pressing (HIP) or pressureless sintering. It can be applied to many advanced materials such as functionally graded materials (FGM), fine ceramics, amorphous materials and nanocomposites.

In the present paper, the in-situ formation of TiB_2 particles in a copper matrix through a combination of mechanical treatment and SHS was investigated. The sintering was also studied using a spark plasma sintering (SPS) process. The microstructures and properties like density, electrical conductivity, hardness and strength of Cu-TiB_2 composites were observed. Additionally wear tests were performed using pin-on-disk wear tester.

Experimental Procedure

Titanium (99.5%, 10 μm, irregular shape), amorphous boron (97%, < 1 μm, irregular shape) and copper (99.5%, 40 μm, rounded) powders were used as starting

*Corresponding author:
Tel : +82-52-259-2244
Fax: +82-52-259-1688
E-mail: jskim@mail.ulsan.ac.kr

materials. Powder mixtures with a stoichiometry of Cu-40%.wt(Ti+2B) were treated in a high energy mill (AGO-2, planetary ball mill type) with a ball acceleration of 600 m/s^2. Balls and vials are made of stainless steel, the diameter of the balls was 5 mm and the powder to ball ratio was 1:20, remaining constant in all experiments. The vials were evacuated and subsequently filled with argon up to 0.3 MPa.

Powder precursors obtained by mechanical treatment were subjected to a SHS-reaction which was ignited by a heating coil of spiral tungsten wire in an argon atmosphere. The SHS-product with 40 wt%TiB_2 was diluted by pure copper powder to obtain the desired composite powders with 2.5, 5 and 10 wt% TiB_2. These composite powders were given a second mechanical treatment to pulverize and distribute the SHS-ed powder homogeneously in the Cu powder. Spark plasma sintering (SPS) was performed in a vacuum using a SPS apparatus (Sumitomo Coal Mining Co. Ltd, AUJ-1611). A graphite mold of 30 mm in inside diameter was used. The applied SPS-pressure and SPS-temperature were 50 MPa and 500-650, respectively. The holding time at the final temperature was 30 minutes. It should be noted that effective temperature of the sample is usually 50 higher than the measured SPS-temperature.

X-ray diffraction patterns (XRD, Cu K_α, Rigaku, RAD-3C) were take for phase analysis of the mechanically alloyed mixtures and SHS-product. The morphology and qualitative analysis (EDS) of powders were observed by means of a field emission-scanning electron microscope (FE-SEM, JEOL, JSM-6500F). The relative density of samples was measured by the Archimedes method and hardness (H_RB) values were measured by a Rockwell hardness tester. Electrical conductivity expressed in %IACS (International Annealed Copper Standard) was measured by a conductivity meter (Fischer, SIMASCOPE® SMP10).

As a comparison, pure copper specimens were also prepared. Tensile specimens cut from the composite are shown in Fig. 1 and tensile tests were conducted at room temperature in a tensile testing machine at a cross-head speed of 0.25 mm minutes^{-1}. Vickers hardness tests were performed at a load of 200g in a digital micro hardness tester.

Dry sliding wear tests were performed in a pin-on-disk wear tester with the composite pin rubbing against a medium carbon steel disk (SM45C). The pin specimen was 5 mm in diameter and 10 mm in height, and the disk was 80 mm in diameter and 10 mm thick. Wear tests were carried out at a sliding speed of 0.83 m/s, and at loads of 29.4 N and 44.1 N, which correspond to contact stresses of 1.50 MPa and 2.25 MPa respectively. Prior to a wear test, the surface of the disk was polished with 800 grit emery paper and cleaned with alcohol and dried. The roughness of the disk surface was approximately 0.5 μm(R_a). When the sliding distance became the designated value(250 m at 59 N and 125 m at 88 N), the weight loss of the specimen was measured with an analytic balance. In order to take the repeatability into account, the test results for wear rate under steady state sliding wear were obtained from the average of three readings.

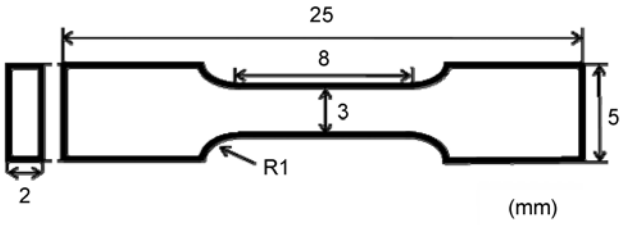

Fig. 1. Small specimen for a tensile test.

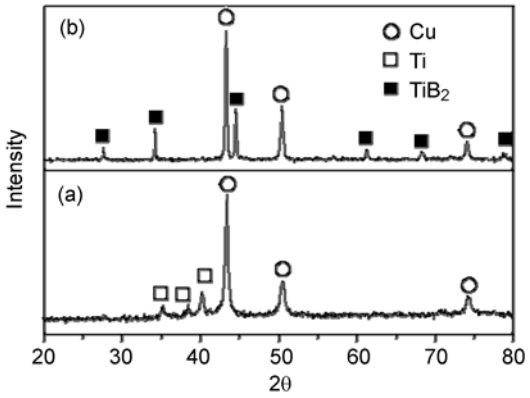

Fig. 2. XRD patterns of powder the (a) preliminary mechanical alloying for 2 minutes and (b) after subsequent SHS-reaction.

Results and Discussion

Figure 2(a) and (b) show XRD patterns of powders after preliminary mechanical alloying for 2 minutes and the subsequent SHS-reaction. No phase formation occurs during the short-time mechanical treatment. X-ray peak broadening indicates a reduction of the grain size and internal strain. The mechanical treatment is of crucial importance for the microstructure formation during SHS. The reagents are plastically deformed and reduced during the treatment so that intimate contact between particles of the reagents and the matrix is achieved This results in a dramatic decrease in the combustion temperature compared to that in untreated mixtures [16] and in the mixture treated for 2 minutes. The decreased combustion temperature favors the formation of fine particles of the product. In the SHS-product, Cu and TiB_2 diffraction peaks are detected. No unreacted reagents remained in the composite. Figure 3 shows the microstructure of the Cu-40 wt.%TiB_2 composite powder produced by the SHS reaction. TiB_2 particles smaller than 250 nm in size are formed by the SHS-reaction between titanium and boron. The TiB_2 particles are homogeneously distributed in the copper matrix. It's observed that the shape of TiB_2 particles,

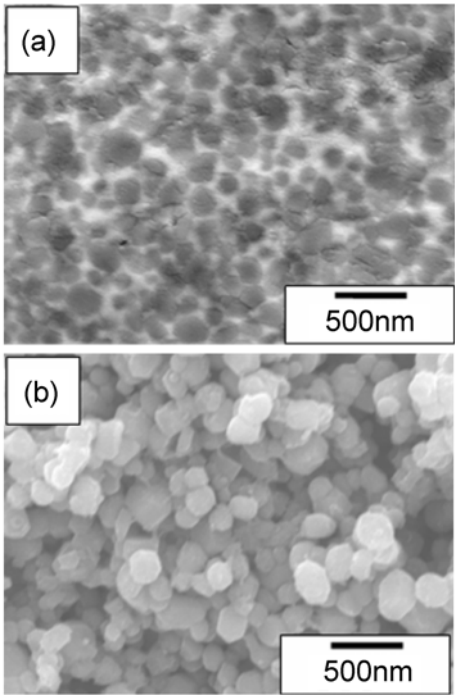

Fig. 3. SEM images of cross-section of SHS-ed powder (a) before and (b) after etching.

confirmed by EDS analysis, is polyhedral after etching.

Spark Plasma Sintering was chosen for compaction because of its advantages for sintering nanostructured materials [17]. Indeed, according to the above considerations the size of TiB_2 particles should be retained during sintering.

Bright and dark areas can be distinguished in the microstructure (Fig. 4(a) and (b)). The dark area is the

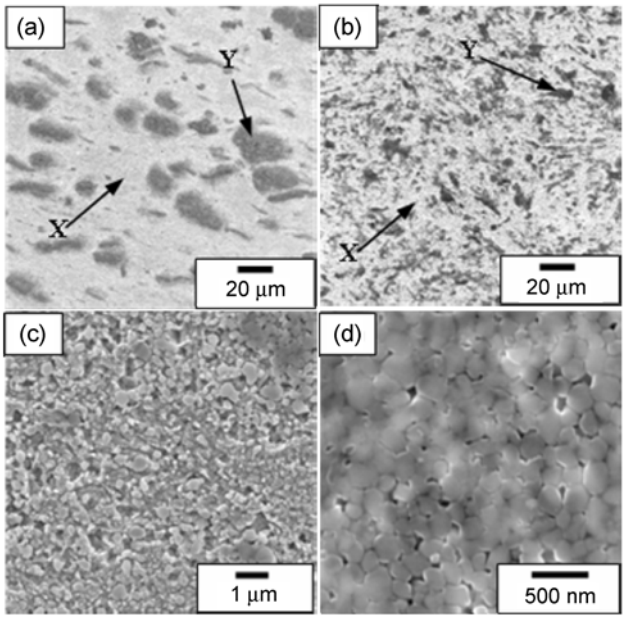

Fig. 4. SEM images of (a) Cu-2.5wt.%TiB_2 and (b) Cu-10 wt.%TiB_2 compacts spark-plasma sintered at 650 °C for 30 minutes and (c) bright and (d) dark area in Cu-2.5wt.%TiB_2 composite.

Table 1. Relative density, hardness and electrical conductivity of Cu-TiB_2 compacts spark-plasma sinteed as a function of sintering temperature and TiB_2 content

TiB_2 content (wt.%)	Sintering temperature (°C)	Holding time (min)	Relative density (%)	Hardness, (H_RB)	Electrical conductivity (%IACS)
2.5	500	30	93.4	54.7	73
2.5	550	30	95.2	55.0	75
2.5	600	30	95.2	56.8	75
2.5	650	30	95.5	56.5	75
5	500	30	90.3	46.4	62
5	550	30	94.0	61.1	66
5	650	30	95.2	62.7	65
10	650	30	93.2	93.1	45

particles of SHS-products. Elemental compositions of bright and dark areas were analyzed by EDS. Peaks corresponding to Cu, Ti, B were found in both areas, however, the intensity of Ti and B peaks was higher in dark areas. This result shows that the particles of the SHS-product were crushed and TiB_2 particles were dispersed in the matrix during milling (Fig. 4(c)). However, the large particles of the SHS-product are still present in the microstructure (Fig. 4(d)). The behavior of SHS-product particles is dependent upon the composition of the composite. The size of the aggregates of titanium diboride particles is smaller in compositions of higher titanium diboride content. It turns out that a lower copper content creates better conditions for breaking the SHS-product particles. So, in case of a higher titanium diboride content the dispersion of the particles of the SHS-product is more effective and, consequently, the distribution of titanium diboride particles in the final composite is more uniform.

Table 1 shows the variation of relative density, hardness and electrical conductivity with sintering temperature and TiB_2 composition. Relative density decreases slightly from 95.5 to 93.2% with increasing TiB_2 content from 2.5 to 10 wt% after SPS at 650 °C. Hardness increases with an increase of TiB_2 content. When compared to specimens sintered at 650 °C, the hardness increases drastically from 56.5 to 97.4 H_RB. The electrical conductivity of sintered specimens decreased with an increase TiB_2 content. Specimens sintered at 650 °C exhibit an electrical conductivity ranging from 75 to 45% IACS (International Annealed Copper Standard). For the same TiB_2 content, there is not a substantial difference in electrical conductivity due to the sintering temperature. The decrease of electrical conductivity is due to the interface scattering of electrons and the fraction of TiB_2 interfaces with increasing TiB_2 content.

The mechanical properties of the composites are given in Table 2. The ultimate tensile strength (UTS), Young's modulus (E) and 0.2 offset yield strength increase as the content of TiB_2 reinforcement increases. The increase in yield strength compared to the pure

Table 2. Tensile properties of Cu-TiB_2 compacts spark-plasma sintered 650°C for 30 minutes

TiB_2 content (wt.%)	0	2.5	5	10
Yield strength (MPa)	233	294	301	369
Ultimate Tensile strength (MPa)	309	366	371	397
Young's modulus (GPa)	121	137	142	155
Elongation (%)	8.5	3.5	1.2	1.1

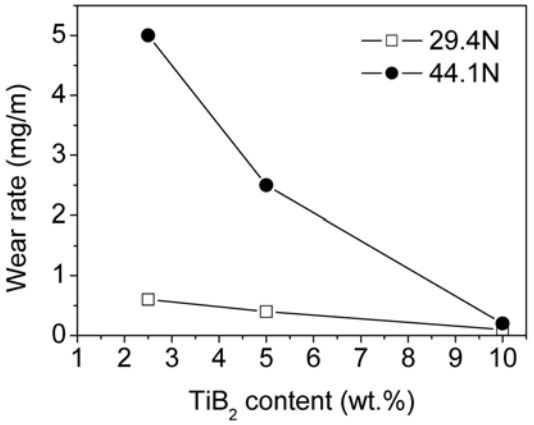

Fig. 5. Variation of wear rate of the Cu-TiB_2 composites with the content of the TiB_2.

copper compact can be attributed to dispersion strengthening by TiB_2 nanoparticles in the Cu matrix It is seen that the elongation of the specimens decreases as the content of reinforcement increases.

Figure 5 shows the variation of the wear rate for the Cu-TiB_2 nanocomposites with TiB_2 content at loads of 29.4 N and 44.1 N. This shows that the wear rates of all the specimen decrease with an increase of the TiB_2 content under dry sliding conditions. It also can be seen that as the load increases the decrease in the rate of wear becomes larger. Although the wear rate of the pure Cu was much higher than the nanocomposites, the wear debris was not detached from the specimen, so the weight loss could not be measured. This is the reason why the data for the Cu is not included in Fig. 5. The results of this work are consistent with the results of the work by Tu et al. [18]. Some other investigators [19-22] found that the sliding wear resistance decreased with an increase the reinforcement concentration under higher applied loads. This deterioration in the wear resistance has been attributed to an increase in reinforcement breakage, reinforcement pull out and poor reinforcement-matrix interfacial bonding.

If the bonding between the matrix and TiB_2 nanoparticles is weak, the TiB_2 reinforcement can be easily pulled out and the wear rate increases.

In this work, the wear resistance of the Cu-TiB_2 nanocomposites increased considerably with the content of TiB_2 nanopaticles within the applied load range. Therefore it can be concluded that the interfacial bond strength does not decrease with an increase the TiB_2 content.

Conclusions

Cu-40 wt%TiB_2 nanocomposite powders were successfully synthesized by a combination of mechanical alloying and a subsequent self-propagating high-temperature reaction. TiB_2 nanoparticles less than 250 nm in size were found to be distributed homogeneously in the Cu matrix.

Samples sintered by SPS had high densities, where the relative density of the Cu-2.5 wt%TiB_2 composite was about 96% of theoretical density. The hardness of Cu-TiB_2 nanocomposites increased, with an increase of the TiB_2 content from 57 H_RB for Cu-2.5 wt%TiB_2 to 97 H_RB for Cu-10 wt% TiB_2, while the electrical conductivity decreased from 75 to 45% IACS. Due to their reinforcement, the yield strength, tensile strength and Young's modulus of the Cu-TiB_2 nanocomposite were significantly improved. Within the applied load range, the wear resistance of the Cu-TiB_2 nanocomposites increased considerably with an increase in the content of TiB_2 nanoparticles.

Acknowledgments

This work was supported by the the Ministry of Commerce, Industry, and Energy (MOCIE), KOREA through the Research Center for Machine Parts and Materials Processing (REMM) at the University of Ulsan.

References

1. M.A. Morris and D.G. Morris, Acta Metall. 35 (1987) 2511-2522.
2. D.G. Morris and M.A. Morris, Mater. Sci. Eng. A 104 (1988) 201-213.
3. J.B. Correia, H.A. Davies, and C.M. Sellars, Acta Mater. 45 (1997) 177-190.
4. A. Upadhyaya and G.S. Upadhyaya, Mater. Design 16 (1995) 41-45.
5. S.E. Broyles, K.R. Anderson, J.R. Groza, and J.C. Gibeling, Metall. Mater. Trans. A. 27 (1996) 1217-1228.
6. Y.Z. Wan, Y.L. Wang, G.X. Cheng, H.M. Tao, and Y. Cao, Powder Metall. 141 (1998) 59-63.
7. S.Y. Chang and S.J. Lin, Scripta Mater. 35 (1996) 225-231.
8. P. Yih and D.D.L. Chung, J. Mater. Sci. 31 (1996) 399-406.
9. J. Pelleg, M. Ruhr, and M. Ganor, Mater. Sci. Eng. A 212 (1996) 139-148.
10. C. Sauer, T. Weissgaerber, W. Puesche, G. Dehm, J. Mayer, and B. Kieback, Int. J. Powder Metall. 33 (1997) 45-53.

11. C. Sauer, T. Weissgaerber, G. Dehm, J. Mayer, W. Puesche, and B. Kieback, Z. Metallkd. 89 (1998) 119-125.
12. C. Biselli, D.G. Morris, and N. Randall, Scripta Metall. Mater. 30 (1994) 1327-1332.
13. G.V. Samsonov and B.A. KovenskayaIn, in Boron and Refractory Borides (ed. V.I. Matkovich), Springer-Verlag, New York, 1977, 19-30.
14. Z.A. Munir, Ceram Bull 67 (1988) 342-349.
15. M. Tokita, J. Soc. Powd. Tech. Japan 30[11] (1993) 790-804.
16. Y.S. Kwon, D.V. Dudina, M.A. Korchagin, O.I. Lomovsky, and H.S. Kim. J. Metastable and Nanocrystalline Materials 15-16 (2003) 253-258.
17. J.R. Groza, and A. Zavaliangos, Mater. Sci. 5[1] (2003) 24-33.
18. J.P. Tu, W. Rong, S.Y. Guo, and Y.Z. Yang, Wear 255 (2003) 832-835.
19. J.P. Tu, L. Meng, and M.S. Liu, Wear 220 (1998) 72-79.
20. J.P. Tu, L. Meng, and M.S. Liu, Wear 2 (1892) 68-73.
21. N. Saka and D.P. Karalekas, Proceeding of the international Conference on Wear of Materials, Canada (1985) 784-793.
22. A.T. Alpas and J.D. Embury, Script Metall. Mater. 24 (1990) 931-935.